Novel gemcitabine conjugated albumin nanoparticles: a potential strategy to enhance drug efficacy in pancreatic cancer treatment

Varun Kushwah, [1,2,3]

Ashish Kumar Agrawal, [1,2]

Chander Parkash Dora, [1]

David Mallinson, [3]

Dimitrios A. Lamprou, [3,4]

Ramesh C. Gupta, [2]

Sanyog Jain, [1]✉

Phone +91-172-2292055
Email sanyogjain@niper.ac.in
Email sanyogjain@rediffmail.com

[1] Centre for Pharmaceutical Nanotechnology, Department of Pharmaceutics, National Institute of Pharmaceutical Education and Research, SAS Nagar, Punjab, India AQ1

[2] James Graham Brown Cancer Centre, University of Louisville, Louisville, Kentucky, USA

[3] Strathclyde Institute of Pharmacy & Biomedical Sciences (SIPBS), University of Strathclyde, Cathedral Street, Glasgow, G4 0RE UK

[4] Medway School of Pharmacy, University of Kent, Medway Campus, Anson Building, Central Avenue, Chatham Maritime, Chatham, Kent, ME4 4TB UK

Abstract

Purpose

The present study reports a novel conjugate of gemcitabine (GEM) with bovine serum albumin (BSA) and thereof nanoparticles (GEM-BSA NPs) to potentiate the therapeutic efficacy by altering physicochemical properties, improving cellular uptake and stability of GEM.

Methods

The synthesized GEM-BSA conjugate was extensively characterized by NMR, FTIR, MALDI-TOF and elemental analysis. Conjugation mediated changes in structural conformation and physicochemical properties were analysed by fluorescence, Raman and CD spectroscopy, DSC and contact angle analysis. Further, BSA nanoparticles were developed from BSA-GEM conjugate and extensively evaluated against *in-vitro* pancreatic cancer cell lines to explore cellular uptake pathways and therapeutic efficacy.

Results

Various characterization techniques confirmed covalent conjugation of GEM with BSA. GEM-BSA conjugate was then transformed into NPs via high pressure homogenization technique with particle size 147.2 ± 7.3, PDI 0.16 ± 0.06 and ZP -19.2 ± 1.4. The morphological analysis by SEM and AFM revealed the formation of smooth surface spherical nanoparticles. Cellular uptake studies in MIA PaCa-2 (GEM sensitive) and PANC-1 (GEM

resistant) pancreatic cell lines confirmed energy dependent clathrin internalization/endocytosis as a primary mechanism of NPs uptake. *In-vitro* cytotoxicity studies confirmed the hNTs independent transport of GEM in MIA PaCa-2 and PANC-1 cells. Moreover, DNA damage and annexin-V assay revealed significantly higher apoptosis level in case of cells treated with GEM-BSA NPs as compared to free GEM.

Conclusions

GEM-BSA NPs were found to potentiate the therapeutic efficacy by altering physicochemical properties, improving cellular uptake and stability of GEM and thus demonstrated promising therapeutic potential over free drug.

Graphical Abstract

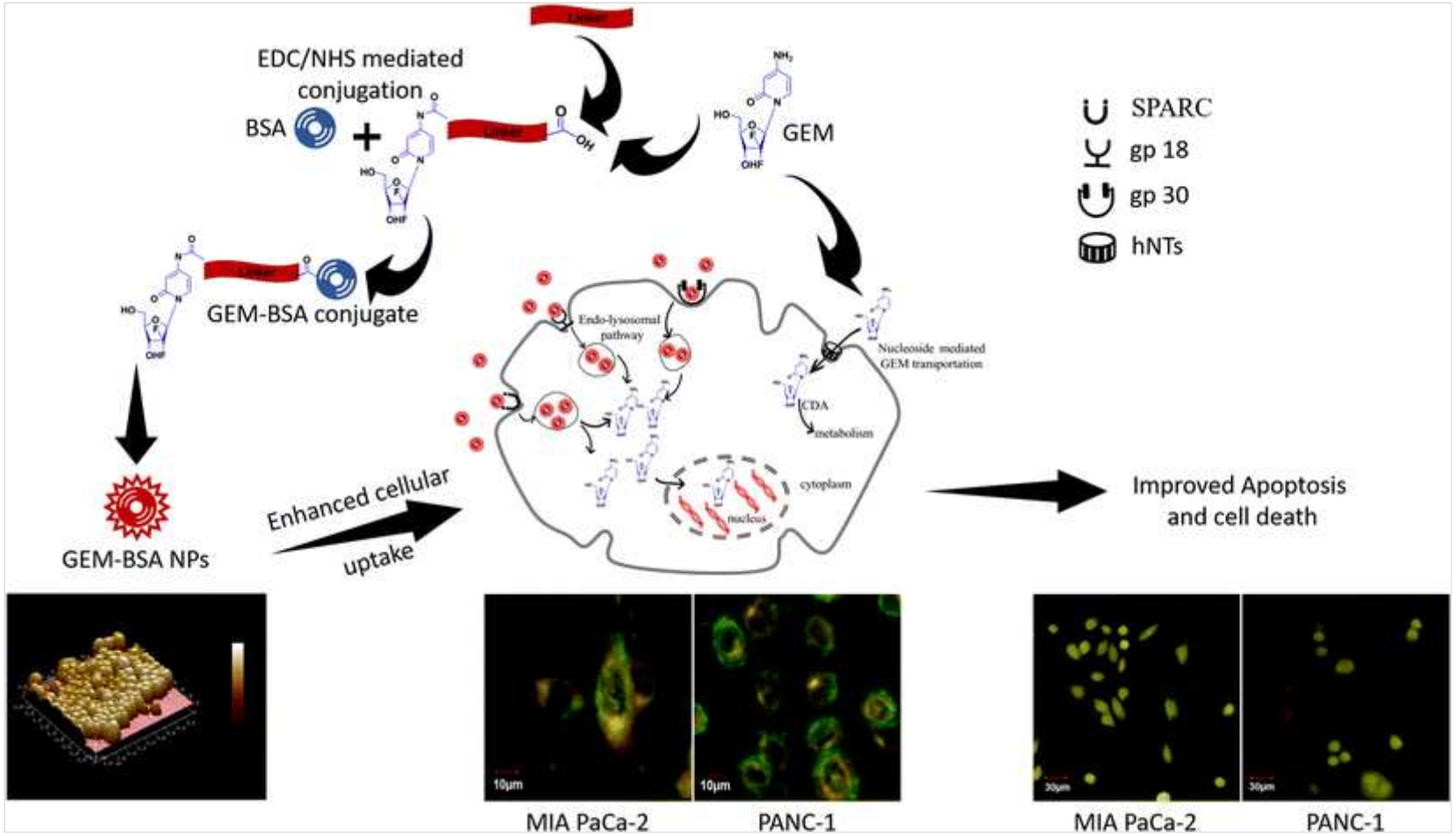

KEY WORDS

BSA nanoparticles
conjugate
gemcitabine
MIA PaCa-2
PANC-1

ABBREVIATIONS

6-CFDA	6-carboxyfluorescein diacetate
8-OHdG	8-hydroxyguanosine
AFM	Atomic force microscopy
AnnCy3	Annexin V-Cy3.18 conjugate
BSA	Bovine serum albumin
C-6	Coumain-6
CD	Circular dichroism
CDA	Cytidine deaminase
CLSM	Confocal laser microscope
CNTs	Human concentrative nucleoside transporters
dFdU	2′,2′-difluorodeoxyuridine
DMEM	Dulbecco’s Modified Eagle Medium
DMSO	Dimethyl sulfoxide
DSC	Differential scanning calorimetry
EDC	1-Ethyl-3-(3-dimethylaminopropyl) carbodiimide
EDTA	Ethylene diamine tetra acetic acid
ENTs	Human equilibrative nucleoside transporters
FBS	Fetal bovine serum
FTIR	Fourier transform infrared
GEM	Gemcitabine
GEM-BSA NPs	Gemcitabine-Bovine serum albumin nanoparticles
HBSS	Hank’s Buffered Salt Solution
hNTs	human nucleoside transporters NMR: Nuclear magnetic resonance
MALDI-TOF	matrix assisted laser desorption ionization time of flight
MTT	3-(4,5-dimethylthiazol-2-yl)-2,5-diphenyltetrazoliumbromide

NHS	N-Hydroxysuccinimide
PDI	Polydispersity index
PXRD	Powder X-ray diffraction analysis
SDS-PAGE	Sodium dodecyl sulfate polyacrylamide gel electrophoresis
SEM	Scanning electron microsc opy
SPARC	Secreted protein acid rich in cysteine
TGA	Thermogravimetric analysis
TNBS	2,4,6-trinitrobenzenesulfonic acid

Electronic supplementary material

The online version of this article (doi: 10.1007/s11095-017-2238-8) contains supplementary material, which is available to authorized users.

INTRODUCTION

Gemcitabine (GEM; 2′, 2′-difluoro-2′-deoxycytidine) is a pyrimidine antimetabolite approved by the Food and Drug Administration (FDA) for the treatment of pancreatic, breast, non-small cell lung and ovarian cancer. It has also shown promising pharmacodynamic potential against brain, bladder and urothelial cancer (1–4). However, the clinical benefits of GEM are limited due to its extremely high hydrophilicity and polarity, which results in unsuitable pharmacokinetics and poor cellular penetration (5). Moreover, therapeutic efficacy is compromised due to its very short half-life (8–17 min) owing to its extensive metabolic degradation via cytidine deaminase, into its water soluble inactive metabolite 2′,2′-difluorodeoxyuridine (dFdU) in blood, liver, and tumors (6). Consequently, a high dose and dosing frequency is required, which further results into dose dependent myelosuppression, nephrotoxicity or haemolytic uremic syndrome. Moreover, GEM exhibits nucleoside mediated transportation across the cellular membrane via human equilibrative nucleoside transporters (ENTs) and human concentrative nucleoside transporter (CNTs). Consequently, a decreased expression of different nucleoside transporters expressions, such as hENT1, results into significantly reduced uptake of gemcitabine into cells, which is the rate limiting step towards its cellular cytotoxicity in GEM resistant cancers (7).

To mitigate above mentioned limitations, several novel drug delivery approaches such as liposomes, chitosan nanoparticles, conjugation and prodrug based approaches have been exploited. Among the various approaches, polymer-anticancer drug conjugates are extensively explored to effectively deliver the hydrophilic drugs to the tumor premises (8–11). The polymeric (PEGylated) conjugates of the GEM have been reported to increase the drug stability by modifying its 4-(N) position with –COOH groups of the polymer through a hydrolysable amide linkage, to protect deamination from cytidine deaminase (CDA), increase plasma half-life and reduces non-specific drug toxicity of GEM on normal tissue by preventing *in vivo* random dissemination of the drug (12–15). In-spite of the promising in-vivo efficacy, the market potential of the reported formulations was hindered owing to application of expensive excipients/carriers, such as PEG, and solvent system for the purification of drug-polymer prodrug. Thus, there is an urge to develop cost effective GEM formulation, with a prospective of translational research.

In the present report, we have hypothesized the conjugation of GEM with BSA and thereof self-assembled nanoparticles will augment the therapeutic efficacy by enhanced permeation and retention effect. Moreover, GEM modified albumin NPs may facilitate its transportation by following the secreted protein acid rich in cysteine (SPARC) mediated endothelial transportation and cellular uptake, as compared to nucleoside transporters followed by free GEM (16).

EXPERIMENTAL METHODS

Chemical and reagents

Gemcitabine was obtained as gift sample from Fresenius Kabi Oncology Limited, Gurgaon, India. BSA, Dimethyl sulfoxide (DMSO) were purchased from Fischer Scientific (USA). N-Hydroxysuccinimide (NHS), 1-Ethyl-3-(3-dimethylaminopropyl) carbodiimide (EDC), Pyridine, Acetic anhydride, Succinic anhydride, fetal bovine serum (FBS), Dulbecco's Modified Eagle Medium (DMEM), 3-(4,5-dimethylthiazol-2-yl)-2,5-diphenyltetrazolium bromide (MTT), antibiotic–antimycotic solution, Triton X-100, ethylene diamine tetra acetic acid (EDTA) were purchased from Sigma. Ultrapure deionized water (LaboStar Ultrapure Water Systems, Germany) was used for all the experiments. All other reagents used were of analytical grade.

Synthesis of GEM-BSA Conjugate

The synthesis of GEM-BSA conjugate is described in three steps: (1) preparation of acetylated intermediate of GEM for the protection of hydroxyl groups, (2) preparation of succinylated intermediate of GEM, (3) covalent conjugation of active succinylated GEM NHS ester with BSA. (Please refer supplementary information).

Characterization of GEM-BSA conjugate

MALDI-TOF analysis

The matrix assisted laser desorption ionization time of flight (MALDI-TOF) mass spectroscopy (Shimadzu, Axima-CFR spectrometer, mass range 1–150,000 Da) was performed for the evaluation of molecular wieght of native BSA and GEM-BSA conjugate. Briefly, 0.5 mg of GEM-BSA conjugate was dissolved into 1 mL of deionized water and mass spectra were recorded.

SDS gel electrophoresis

The molecular weight of the BSA and GEM-BSA conjugate were further analysed by sodium dodecyl sulfate polyacrylamide gel electrophoresis (SDS-PAGE) (17). Briefly, BSA and BSA-GEM conjugate ~5 mg were dissolved in 1 mL distilled water and analysed by BCA kit (Thermo Scientific, Rockford, IL) for protein determination. The BSA and GEM-BSA conjugate were compared in triplicate against standard BSA solution as per standard manufacturer’s instructions. Thereafter, equal amount of proteins was loaded in the individual well and further electrophoresed at 200 V for 30 min. The resolved bands were visualized by staining with Coomassie blue.

Elemental analysis

Elemental analysis was carried out with Flash 2000 Organic elemental analyser (Thermo Scientific). About 5 mg of sample was taken in a tin boat and analysed using helium as the carrier gas. The spectra of C, N and S were recorded and the elemental compositions of the samples were expressed as atomic percentage.

Circular dichroism (CD) assay

The 3D conformational structure of native BSA and GEM-BSA conjugate was determined using CD spectroscopy (J-815; Jasco, Tokyo, Japan). Different samples (GEM, BSA, BSA-GEM conjugate and GEM-BSA NPs) were placed in rectangular quartz cuvette (0.1 cm path length) and scanned in the far UV region of 260–190 nm to obtain CD spectrum. Each sample was evaluated in triplicate and distilled water was utilized for baseline correction.

Raman spectroscopy

Raman spectra of BSA and GEM-BSA conjugate were obtained using Raman microscope (ThermoScientific, Madison, USA) with a DXR 532 nm laser. All spectra were recorded over a range of 500–1700 cm^{-1} for the analysis of conformational changes (α-helix and ß-sheets) of BSA on conjugation with GEM. The samples were analysed as lyophilized solids at room temperature (25°C).

Differential scanning calorimetry (DSC) and Thermogravimetric analysis (TGA)

Thermal characteristics of GEM, BSA, physical mixture (1:1w/w) and GEM-BSA conjugate were analysed using DSC Mettler Toledo 821e TGA/SDTA (Mettler Toledo, Switzerland). Each sample (3–5 mg) was heated in an aluminium pan between 20–300°C at a scanning rate of 10°C/min under inert nitrogen atmosphere. Empty pan was used for the calibration of heat rate baseline. Further, the GEM immobilized through the carbodiimide chemistry to the BSA was analysed by using thermogravimetric analysis in a range of 20–300°C with heating rate of 10°C/min.

Contact angle and wettability measurements

Sessile drop method was utilized for the evaluation of contact angle of BSA and GEM-BSA conjugate (Drop Shape Analyser, FTA 1000, First Ten Angstrom, Virginia, USA). Samples (GEM, BSA and developed NPs) were fixed on double sided adhesive tape, previously adhered on glass slide. Thereafter, the excess BSA and GEM-BSA conjugate was then removed and a drop of Milli-Q water was placed on the film of samples and observed via FTA image analyser. Contact angle was then evaluated by the instrument via fitting mathematical equations (eq. 1). The surface tension of Milli-Q water was measured to be 73.1 ± 0.5 mN/m and controlled environment condition of 25 ± 2°C/55 ± 5% RH was maintained while preforming experiments.

$$\Upsilon SV\text{--}\Upsilon LS = \Upsilon LS \cos\theta$$

1

Where θ, ϒSV and ϒLS are contact angle, interfacial tension between solid-vapour and interfacial tension between liquid-vapour, respectively.

Preparation of GEM-BSA NPs

GEM conjugated BSA nanoformulations were prepared via high pressure homogenization with slight modification (18). Briefly, 100 mg of GEM-BSA conjugate was solubilized in 10 ml distilled water. To this aqueous phase, 2 ml of 1:1 ratio of ethanol and chloroform was added dropwise (1 ml/min), under a low shear forces (magnetic stirrer) at 1200 rpm and kept for 1 h in order to form crude emulsion. The above emulsion was subjected to high-pressure homogenization (20,000 psi for 9 cycles). Residual chloroform and ethanol were evaporated by rotary evaporation. The aqueous dispersion containing nanoparticles was lyophilized (Please refer supplementary information).

Characterization of GEM-BSA NPs

Particle size and zeta potential

The developed GEM-BSA nanoparticles were assessed for their critical quality attributes such as particle size, polydispersity index (PDI) and zeta potential (ZP) via Zeta Sizer (Malvern Instruments, UK). All measurements were carried out after suitable dilution with HPLC grade water. Final values are presented as the average of 6 measurements.

Shape and Morphology

Shape and morphology of GEM-BSA NPs was evaluated by atomic force microscopy (AFM) and scanning electron microscopy (SEM). AFM was carried out to obtain three-dimensional (3D) surface morphology of the nanoparticles. A Bruker Multimode 8 atomic force microscope with Nanoscope V controller was used for the AFM measurements. Measurements were made in air under ambient conditions iusing the QNM mode. Analysis was obtained using a V-shaped ScanAsyst air probe from Bruker (nominal spring constant 0.4 N m-1; nominal

resonant frequency 70 kHz; nominal length 600 nm). A drop of GEM-BSA nanoformulation was air dried for ~30 min over the silicon mica and further analysed using AFM.

The surface morphology was further analysed by SEM (S-3400 N, Hitachi, Japan). The SEM analysis was performed by placing a drop of GEM-BSA NPs and BSA NPs over the glass coverslip attached to aluminium stub via bi-adhesive tape. The drop was then kept for air drying for ~30 min and observed using SEM at 10 kV.

Powder X-ray diffraction analysis (PXRD)

PXRD spectra of GEM, BSA, Mannitol (MT), Physical mixture (equal mixture of GEM, BSA and MT) and GEM-BSA conjugate were recorded by X-ray diffractometer (D8 Advanced Diffractometer, Bruker AXS GmbH, Germany). The X-ray source was Cu Kα tube (wavelength 1.5406 Å) operated at 40 kV and 40 mA. The samples were scanned from 4° to 40° (2θ at a scan rate of 0.1° (2θ) /min). The diffractograms were further analysed with software DIFFRAC plus EVA (ver.9.0).

In-vitro release studies

The *in-vitro* hydrolytic stability of the developed GEM-BSA NPs was assessed to evaluate the rate of GEM release from GEM-BSA NPs in phosphate buffered saline (PBS) (pH 5.5 and pH 7.4). Moreover, the effect of crude protease on the stability of conjugate was also studied. Briefly, NPs (equivalent to 100 µg/mL of GEM) was taken in a dialysis bag (molecular weight cut-off 1000 Da) was added in PBS at pH 5.5 and 7.4, respectively at 37 ± 0.1°C. At predetermined time intervals, aliquots (1 mL) were withdrawn and replaced with an equivalent amount of the fresh PBS and further analysed for the amount of GEM released from the GEM-BSA NPs via validated HPLC method (please refer supplementary information).

In-vitro cell culture experiments

Cells

Human pancreatic cancer cell lines (MIA PaCa-2 and PANC-1) were purchased from National Centre for Cell Sciences (NCCS), India and were grown in tissue culture flasks (75 cm^2) at 5% CO_2 and temperature 37°C. The medium comprised of Dulbecco's Modified Eagle Medium (DMEM) with 10% FBS, 100 U/mL penicillin, and

100 μg/mL streptomycin (PAA Laboratories GmbH, Austria) for both MIA PaCa-2 and PANC-1 and was changed on every alternate day. The cultured cells were trypsinized after reaching the 90% confluency with 0.25% trypsin-EDTA solution. For qualitative cell uptake analysis, MIA PaCa-2 and PANC-1 cells were then seeded (50,000 cells/well) in 6-well cell culture plates (Costars, Corning Inc., NY, USA) and observed under confocal laser microscope (CLSM) (Olympus FV1000). Moreover, for MTT assay, MIA PaCa-2 and PANC-1 cells were seeded (10,000 cells/well) in 96 well cell culture plates (Costars, Corning Inc., NY, USA).

Cell uptake and internalization studies

Cell uptake and internalization pathways of GEM-BSA NPs were evaluated as per previously published reports with slight modifications (19). MIA PaCa-2 and PANC-1 cells were cultured onto a 6-well plate as described above. Coumain-6 (C-6; model dye for cellular uptake analysis) loaded GEM-BSA NPs were prepared by method mentioned above, except C-6 was dissolved in organic phase (1:1 ratio of ethanol and chloroform). Internalization pathways of GEM-BSA NPs were assessed using endocytotic inhibitors including chlorpromazine (clathrin-mediated endocytosis inhibitor) and genistein (caveolae mediated endocytosis inhibitor). The cells were pre-incubated with chlorpromazine (10 mg/mL), genistein (1 mg/mL), and combined treatment with chlorpromazine and genistein to assess the combination effects for 1 h at 37°C (20). After the incubation period, media was replaced with fresh media containing C-6 loaded BSA NPs (equivalent to 1 μg/mL of free C-6) for 2 h. Thereafter, cells were washed three times with Hank's Buffered Salt Solution (HBSS) to remove the extracellular particles and fixed with 3% paraformaldehyde (Merck, India) and observed under CLSM.

Subcellular fate of GEM and GEM-BSA NPs

The intracellular localization of GEM and GEM-BSA NPs into the endo-lysosomal track was determined using LysoTracker (Ex/ Em 577/590 nm) dye specific to the acidic organelles (15). MIA PaCa-2 cells and PANC-1 were treated with GEM and GEM-BSA nanoparticles 10 μg/mL concentration for 24 h. Following treatment, the cells were washed three times with HBSS and further incubated with the media containing 1 μM LysoTracker Red for 30 mins. Thereafter, the cells were again washed thrice using HBSS and fixed with 2.5% *v*/v glutaraldehyde solution. Cells once fixed, were observed by CLSM for red fluorescence.

Nucleoside transporter (hNTs) inhibition

Dipyridamole was utilized as hNTs inhibitor to evaluate the role of hNTs mediated membrane transportation of GEM in case of free GEM and GEM-BSA NPs, during *in-vitro* cytotoxicity assay (21). MTT assay was performed as per the protocol mentioned above with slight modifications. MIA PaCa-2 and PANC-1 (10,000 cells/well) cells were trypsinized and seeded in 96-well cell culture plates for 24 h. Thereafter, the cells were pre-incubated with 10 mM dipyridamole for 30 min prior to addition of free GEM and GEM-BSA NPs at concentrations (0.1, 1, 10, and 20 μg/mL equivalent to free GEM) and IC_{50} was calculated by using CalcuSyn 2.1 software.

Cytotoxicity

MTT assay was employed to determine the cell cytotoxicity of GEM-BSA NPs in MIA PaCa-2 and PANC-1 cell lines by following our previously reported protocol (22). MIA PaCa-2 and PANC-1 (10,000 cells/well) were seeded to 96-well tissue culture plates (Costars, Corning Inc., NY, USA) in a total volume of 200 μL of DMEM media and kept overnight for the attachment of cells. Following the attachment of cells, the media was aspirated and fresh media (200 μL) containing free GEM, GEM-BSA conjugate and GEM-BSA NPs were added at a concentration of 0.1, 1, 10, and 20 μg/mL (equivalent to free GEM) and further incubated for 24, 48 and 72 h. After the incubation period, the media containing formulation was cautiously aspirated and the formazan crystals then solubilized with 200 μL DMSO and the optical density (OD) of the resultant solution measured at 550 nm using an ELISA plate reader (BioTek, USA). The cell viability was evaluated by eq. 2.

$$Relative\ cell\ viability = \frac{Absorbance\ (Sample)}{Absorbance\ (Control)} \quad (2)$$

DNA damage assay

GEM-BSA NPs and free GEM were evaluated for the DNA damage potential via estimation in alterations of 8-hydroxyguanosine (8-OHdG; DNA damage marker) levels (14). Briefly, MIA PaCa-2 and PANC-1 cells were exposed to varying concentrations of GEM and GEM–BSA NPs (0.1, 1, 10 and 20 μg/mL equivalent to GEM). After incubation of 12 h, cells were washed three times with HBSS. The cells were then collected and digested

under anaerobic conditions. Thereafter, 8-OHdG levels were determined using ELISA kit (OxiSelect Oxidative DNA Damage ELISA Kit, STA-320) using manufacturer's instructions with DMSO as a negative control.

Annexin-V apoptosis assay

The cytotoxicity efficacy of the GEM-BSA NPs was also assessed via Annexin-V apoptosis assay as per our previous reports (23). MIA PaCa-2 and PANC-1 cells incubated with GEM, GEM-BSA NPs, equivalent to 10 μg/mL of GEM for 6 h. After incubation, cells were washed three times with HBSS and stained with Annexin V-Cy3.18 conjugate (AnnCy3) and 6-carboxyfluorescein diacetate (6-CFDA) as per the manufacturer's protocol (Annexin V-Cy3™ Apoptosis Detection Kit, Sigma, USA) and observed under red and green fluorescent channel, respectively by CLSM. The cells stained with red, green and yellow (overlap of red and green) fluorescence were considered as necrotic, live and apoptotic, respectively. Furthermore, quantitative estimation of apoptosis was also evaluated via calculating Apoptosis index (ratio of the red and green fluorescence intensity). The fluorescence intensity was quantified by Image J software (U. S. National Institutes of Health, USA).

Statistical analysis

All data have been mentioned as mean ± SD. Statistical analysis was performed with Graph Pad Prism software (version 7.0) using one-way ANOVA, followed by Tukey–Kramer multiple comparison test.

RESULTS

Characterization of GEM-BSA conjugate

MALDI-TOF

GEM-BSA conjugate exhibited significant increase in molecular weight as compared to native BSA (Fig. 1 A). In the case of native BSA, the center of the mass distribution curve was observed at m/z 66,290.92 and 33,343.68, while, after conjugation of BSA with GEM, the centre of the mass distribution curve shifted to m/z ~ 68,767.46 and 35,048.79, respectively.

Fig. 1

(**a**) MALDI-TOF spectra of BSA and GEM-BSA conjugate; (**b**) SDS Page analysis of BSA (lane1) and GEM-BSA (Lane 2); (**c**) Overlay CD spectra of BSA and GEM-BSA conjugate and (**d**) Raman spectra of BSA and GEM-BSA conjugates.

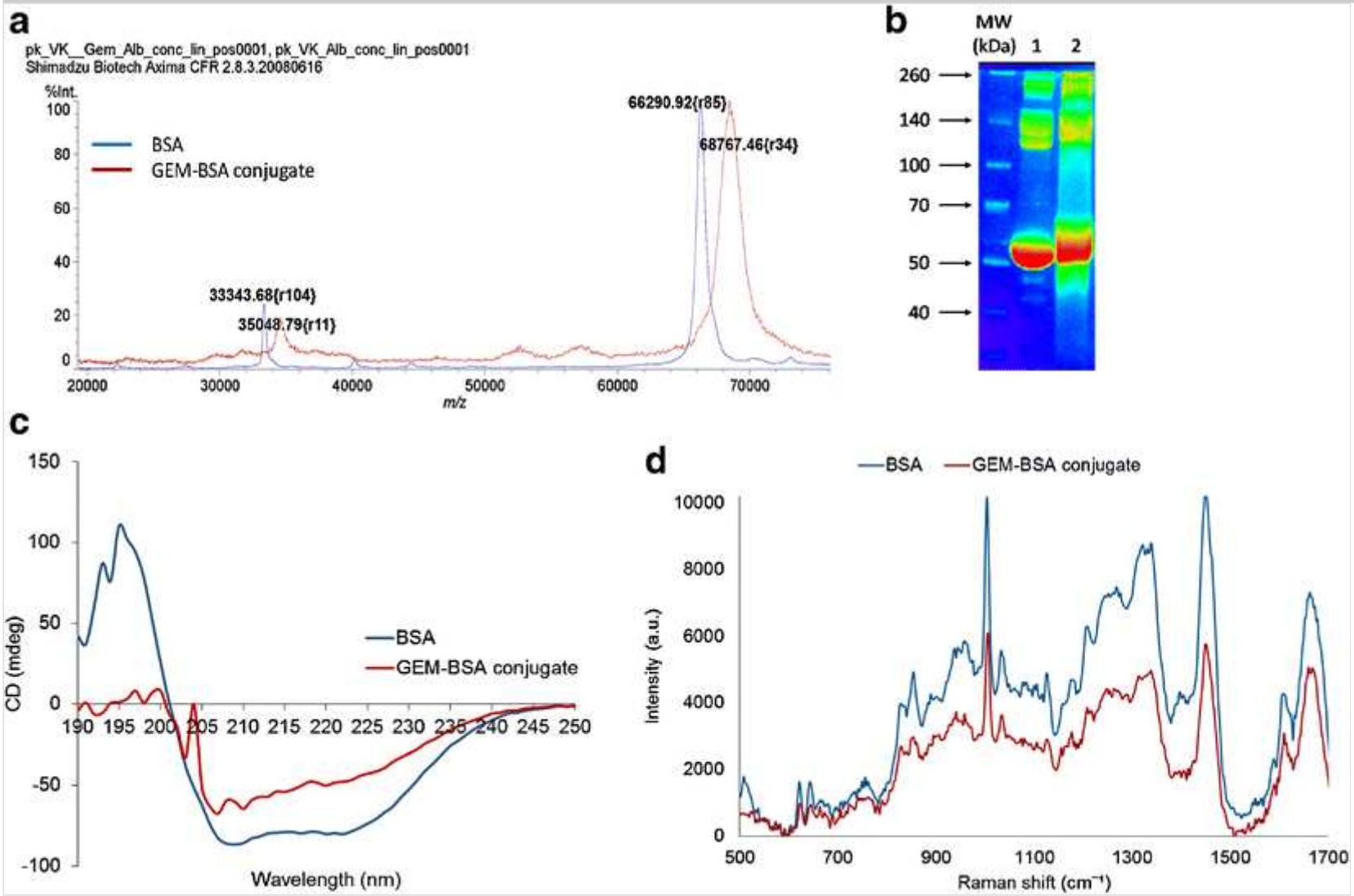

SDS gel electrophoresis

In line with the MALDI-TOF results, SDS-PAGE demonstrated remarkable increase in molecular weight of GEM-BSA in comparison with plain BSA (Fig. 1 B).

Elemental analysis

The compositions of BSA and GEM-BSA conjugate were analysed via elemental analysis summarized in Table I. Elemental analysis of BSA revealed 13.63% (N), 45.18% (C); 7.16% (H) and 1.43% (S), while, elemental composition of GEM-BSA conjugate was 13.90% (N), 47.90% (C); 6.89% (H) and 1.14% (S). The increase in the values of N and C clearly demonstrate the synthesis of GEM-BSA conjugate.

Table I

Percentage Composition of Different Elements Present in Different Samples of BSA and GEM-BSA

S. No.	Name of Sample	Nitrogen %	Carbon %	Hydrogen %	Sulphur %
1	BSA	13.63	45.18	7.16	1.43
2	GEM-BSA	13.90	47.90	6.89	1.14

Circular dichroism (CD) assay

CD spectra of BSA and GEM-BSA are shown in Fig. 1 C. GEM-BSA conjugate demonstrated α helix, ß sheets and turns percentage of 23.1%, 16.4% and 27.0%, while the native BSA demonstrated 26.0%, 30.6% and 17.7%, respectively (Table II).

Table II

Percentage of Structural Components of BSA and GEM-BSA

S. No.	Sample	Helix%	Beta%	Turn%
1.	BSA	26.0	30.6	17.7
2.	GEM-BSA	23.1	16.4	27.0

Raman spectroscopy

Raman spectra of drug albumin conjugates were obtained using Raman microscope (ThermoScientific, Madison, USA) with a DXR 532 nm laser. Figure 1 D depicts the stronger intensities in the amide-III region at 1200–1300 cm^{-1}, amide I region at 1658 cm^{-1}, skeletal stretching region near 900–1000 cm^{-1} and charged amino end groups at 800 and 850 cm^{-1}. were observed in the spectrum of native BSA. A decrease (from 0.676 to 0.539) in intensity ratio of I_{934}/I_{1003} and an increase (from 0.699 to 0.854) in intensity ratio of I_{1246}/I_{1337} were found in case of GEM-BSA as compared to native BSA (Table III).

Table III

Intensity Ratio (I_{934}/I_{1003} and I_{1246}/I_{1337}) of BSA and GEM-BSA in Solid State Raman Spectroscopy

S. No.	Samples	I_{934}/I_{1003}	I_{1246}/I_{1337}
1.	BSA	0.676	0.699
2.	GEM-BSA conjugate	0.539	0.854

Differential scanning calorimetry (DSC) and Thermogravimetric analysis (TGA)

DSC thermogram of GEM and physical mixture of GEM and BSA exhibited an endotherm peak at ~273°C corresponding to GEM, while, BSA, GEM-BSA exhibited broad peaks at 70°C and 220°C (Fig. 2 A). Thus, absence of characteristic peak of GEM depicts the absence of crystalline structure of GEM following the conjugation with the BSA. Furthermore, in TGA analysis (Fig. 2 B) GEM-BSA and BSA demonstrated two phase degradation profile. In the initial phase (first degradation profile) GEM-BSA and BSA exhibited 6.23% and 5.06% initial weight loss from room temperature to ~110°C, respectively. Thereafter, the BSA exhibited a plateau phase (stable towards degradation) from 110°C to 235°C followed by further degradation to 63.14% weight loss, while the GEM-BSA demonstrated a very short stable phase from ~110°C to ~160°C followed by significant higher degradation of 74.51% in comparison with BSA.

Fig. 2

(**a**) Overlay of DSC thermograms of free GEM, BSA, GEM-BSA conjugate and physical mixture of BSA and GEM; (**b**) TGA thermograms of BSA and GEM-BSA conjugate; (**c**) Qualitative contact angle evaluation/ Water droplet profile on films of (*a*) BSA and (*b*) GEM-BSA conjugate; and (**d**) Quantitative estimation of contact angle of BSA and GEM-BSA conjugate.

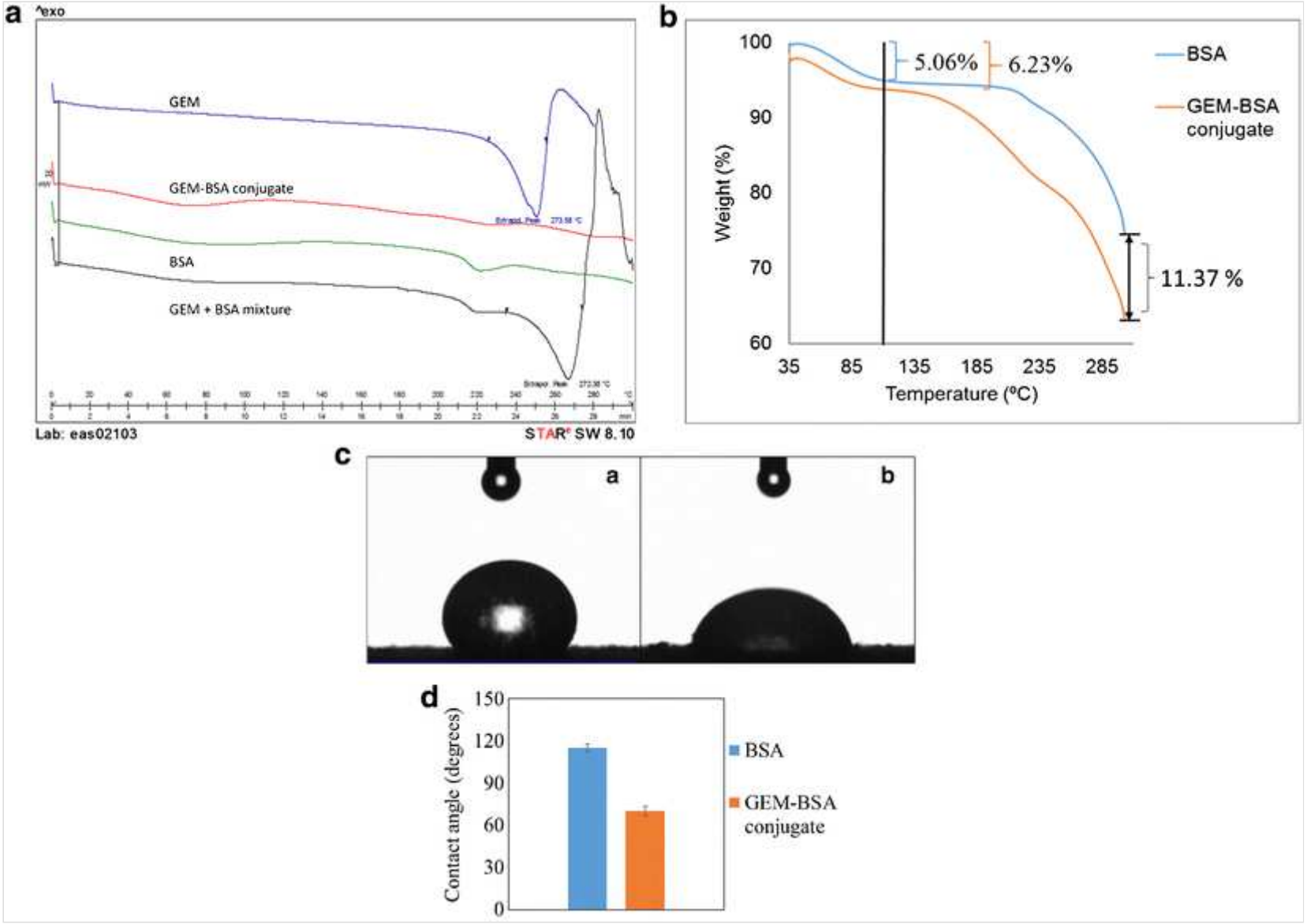

Contact angle and wettability

Wetting behaviour of the developed conjugates was evaluated by measuring the contact angle. The contact angle of the drop was found to be 115.15 ± 2.72° and 70.13 ± 3.57° for native BSA and GEM-BSA conjugate, respectively.

Furthermore, the qualitative water droplet profile with the BSA and GEM-BSA demonstrated the rapid coalescence of the water droplet with the GEM-BSA conjugate powder film as compared to the BSA (Fig. 2 C).

Characterization of GEM-BSA NPs

Shape and Morphology of GEM-BSA NPs

The quality attributes of final optimized formulation GEM-BSA NPs were depicted in Table IV. Further, morphology analysis via SEM and AFM (Fig. 3) affirmed development of smooth and spherical shape nanoformulation, which were found to be in correspondence with DLS results.

Table IV

Particle Size, PDI, ZP and % Drug Loading of GEM-BSA NPs

S. No.	Sample	Particle size (nm)	PDI	ζ (mV)	% GEM loading (mg/100 mg BSA)
1.	BSA NPs	139.3 ± 6.6	0.101 ± 0.04	−34.50 ± 1.65	-
2.	GEM-BSA NPs	147.2 ± 7.3	0.161 ± 0.06	−19.20 ± 1.41	3.23 ± 0.15
Values are presented as mean ± SD (n = 6)					

Fig. 3

Surface morphology analysis via (**a**) SEM image (**b**) AFM image of (*a*) BSA NPs and (*b*) BSA-GEM NPs and (**c**) PXRD diffractogram of GEM, BSA, GEM-BSA conjugate, mannitol, physical mixture (GEM, BSA and Mannitol) and freeze dried GEM-BSA NPs.

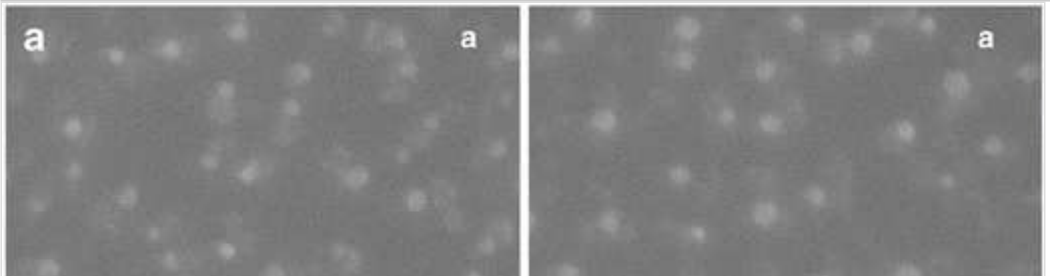

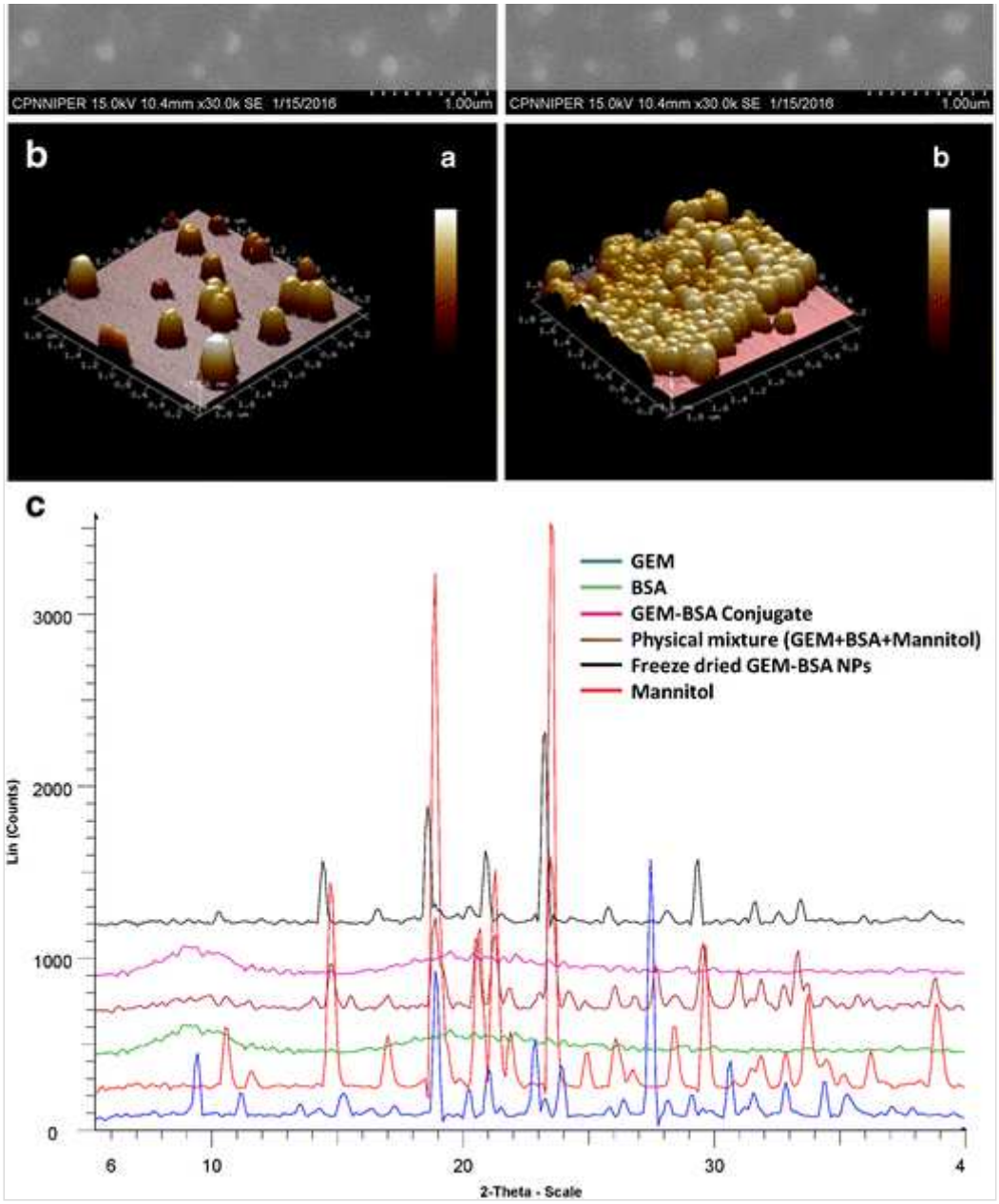

Powder X-ray diffraction analysis (PXRD)

PXRD analysis made it possible to assess the length of the long and short spacing of the crystal lattice of different ingredients. Fig. 3 (C) demonstrated presence of several characteristic diffraction peaks of GEM at 2θ scattered angle of 7.3°, 9.2°, 14.6°, 19.7°, 20.6°, 21.9°, 23.4°, 25.3°, 27.6° in case of free GEM and physical mixture. However, characteristic peaks of GEM were not found in PXRD spectra of GEM-BSA conjugate, which confirmed the conversion of crystallinity of GEM into amorphous state after conjugation with BSA.

In-vitro Release Studies

A sustained release of GEM was evaluated at both the pH conditions (pH 5.5 and 7.4), however the amount of GEM released at pH 7.4 was slightly lower in comparison with GEM released at pH 5.5 (Fig. 4). Interestingly, significant higher amount of GEM was released in presence of protease at both the pH conditions as compared to amount of GEM released in the absence of protease.

Fig. 4

In-vitro release profile of GEM from GEM-BSA conjugate and GEM-BSA NPs at pH (**a**) 7.4 and (**b**) 5.5 in the presence and absence of protease.

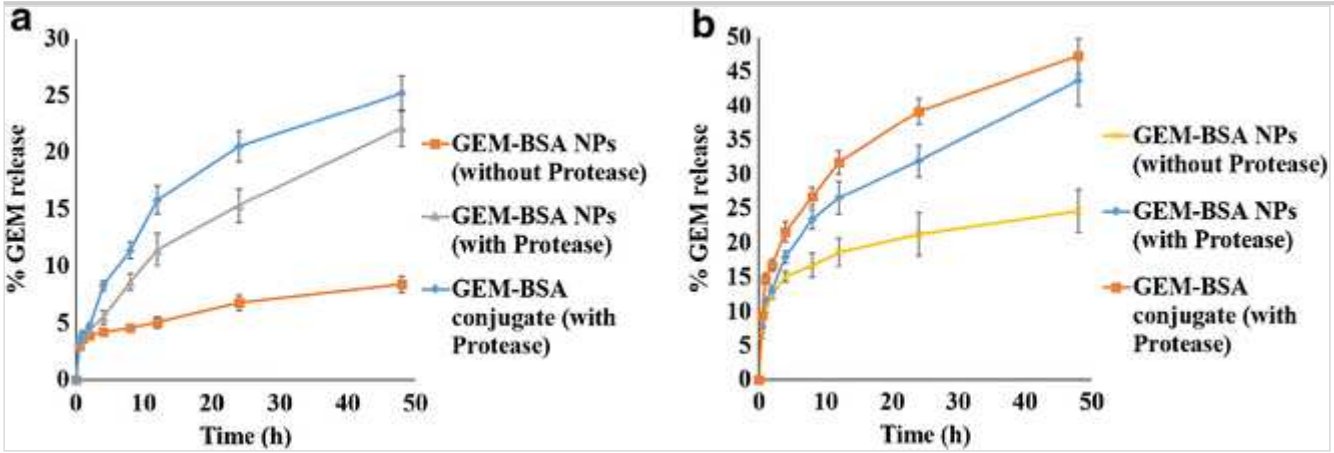

In-vitro cell culture experiments

Cell uptake and internalization pathway of GEM-BSA NPs

C-6 loaded GEM-BSA NPs showed significantly higher uptake in both MIA-PaCa 2 and PANC-1 cells as compared to free C-6 indicative of significantly higher internalization of nanoformulations (Fig. 5 A and B). Further, the internalization pathways of the developed NPs were also investigated. Insignificant reduction of fluorescence intensity was found when the cells were incubated with genistein, an inhibitor of tyrosine kinase mediated caveolae uptake (Fig. 5 C). In contrast, significantly higher reduction in fluorescence intensity was observed when the cells were pre-incubated with chlorpromazine and a combination of chlorpromazine and genistein (Fig. 5 D and E).

Fig. 5

Cell uptake and internalization at a concentration 1 μg/ml for 2 h with (**a**) Free Coumarin-6 (C-6), (**b**) C-6 loaded GEM-BSA NPs (**c**) C-6 loaded GEM-BSA NPs upon pre-incubation of Genistein, (**d**) C-6 loaded GEM-BSA NPs upon pre-incubation of Chlorpromazine, and (**e**) C-6 loaded GEM-BSA NPs upon pre-incubation of combination of Chlorpromazine and Genistein. In all the images, Panel (*a*) Images under the green fluorescence channel; Panel (*b*) Corresponding differential interface contrast images of cells (*c*) Superimposition of panel (*a*) and panel (*b*). Panel (*d*) and (*e*) in all the images show horizontal line series analysis of fluorescence along the white line.

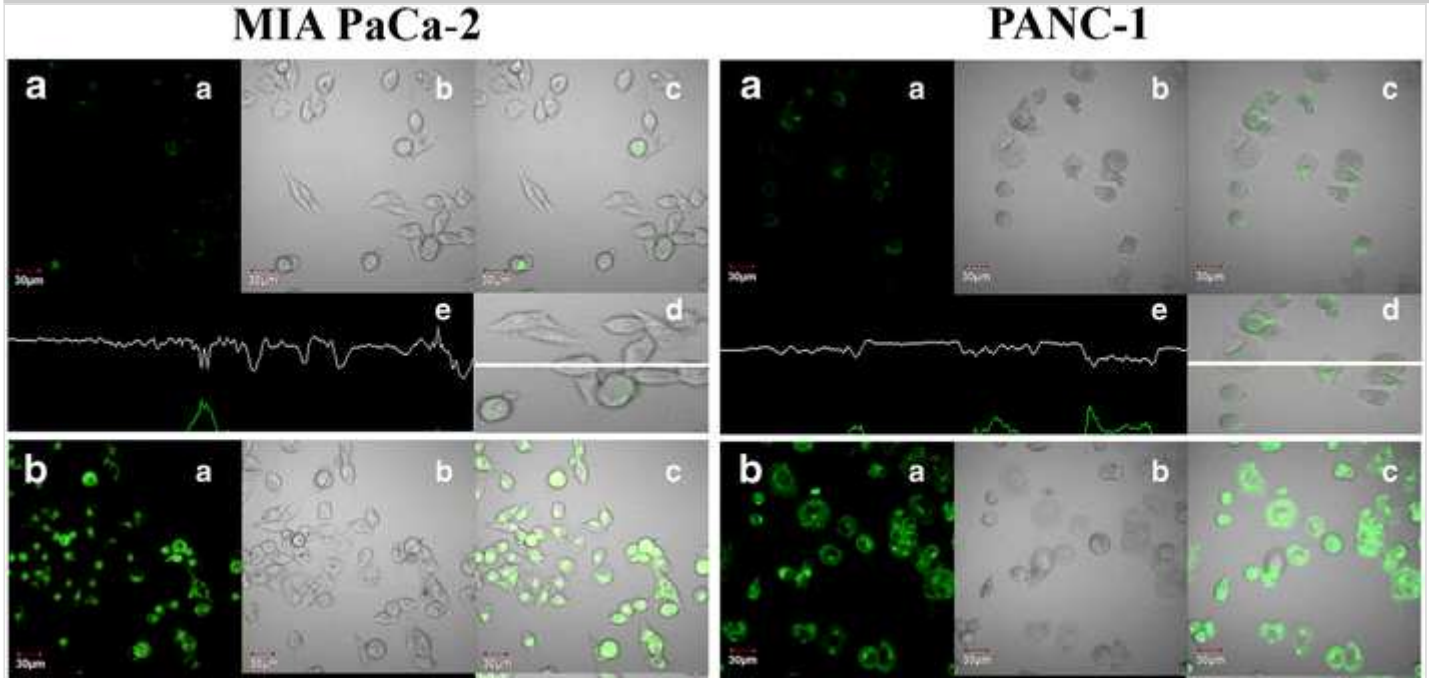

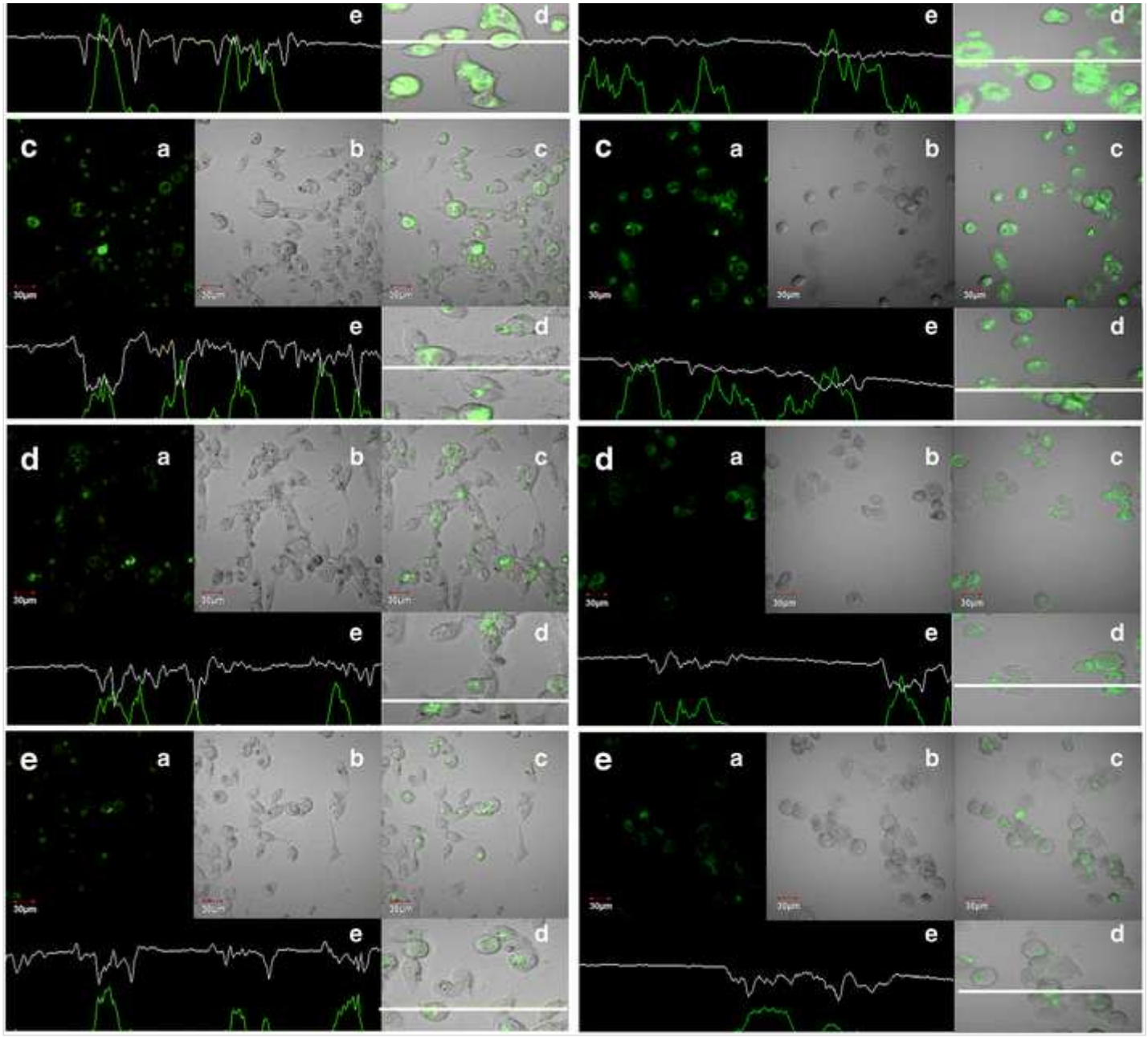

Subcellular fate of GEM and GEM-BSA NPs

Subcellular fate of GEM and C-6 loaded GEM-BSA NPs was evaluated utilizing LysoTracker Red dye. Figure 6 demonstrated relative formation of sub-cellular structures (lysosomes and endosomes) after treatment with GEM and C-6 loaded GEM-BSA NPs for 24 h. Cells incubated with C-6 loaded GEM-BSA NPs, exhibited significantly higher red fluorescence as compared to cells incubated with GEM alone, indicative of higher lysosome or endosome formation in case of NPs treatment. Further, Fig. 6 B demonstrates that the red fluorescence was found to be overlapped with the green fluorescence due to C-6 loaded GEM-BSA NPs in the peripheral part of the cells, which confirms the co-localization of the developed NPs with the lysosomes.

Fig. 6

Intracellular fate of (**a**) GEM and (**b**) GEM-BSA NPs shown by staining with LysoTracker Red after 24 h. Panel (*a*) Images under the red fluorescence channel of LysoTracker; Panel (*b*) Corresponding differential interface contrast images of cells (c) Superimposition of Panel (*a*) and Panel (*b*); Panel (*d*) and (*e*) in all the images show vertical and horizontal line series analysis of fluorescence along the white line; and Panel (*) and (**) depicts green fluorescence channel of C-6 loaded GEM-BSA NPs and overlay of figure (a) and (*), respectively.

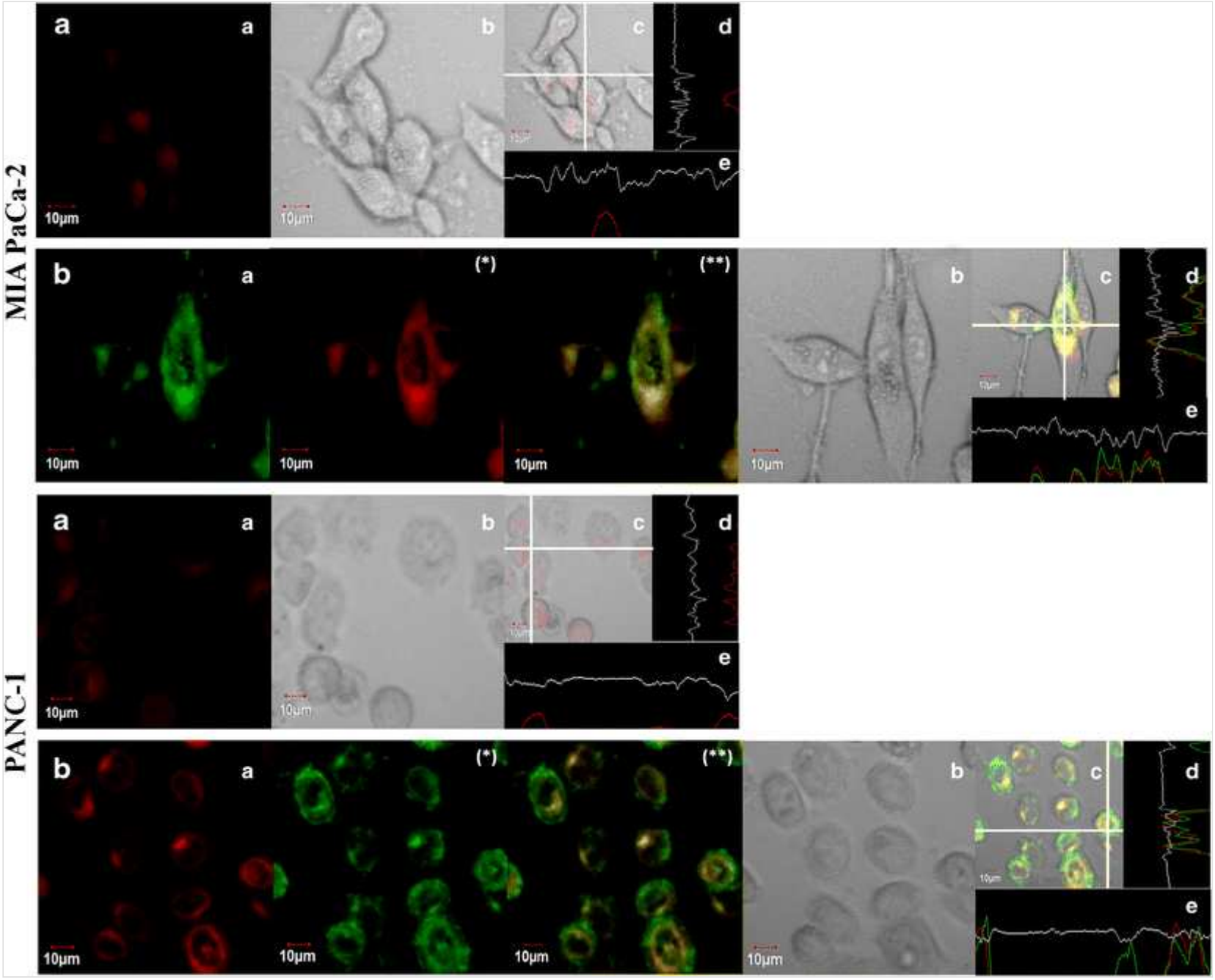

Nucleoside transporter (hNTs) inhibition

Nucleoside transporter inhibition study was performed to investigate the dependence of GEM and GEM-BSA NPs on the human nucleoside transporters for their therapeutic effect. MIA-PaCa 2 and PANC-1 cell lines were incubated with dipyridamole (a nucleoside transporter inhibitor), before the treatment with GEM and GEM-BSA NPs. Thereafter, the IC_{50} values were obtained for GEM and GEM-BSA NPs in the absence and presence of dipyridamole. MIA-PaCa-2 and PANC-1 exhibited IC_{50} value 8.47 and 9.27 folds greater, when GEM treated cells were pre-incubated with the dipyridamole as compared to cells devoid of dipyridamole, however this difference was insignificant in case of GEM-BSA NPs. MIAPaCa-2 and PANC-1 cell line expressed significant reduction of sensitivity towards GEM when treated with dipyridamole, while sensitivity was not altered in case of GEM-BSA NPs (Table V).

Table V

Effect of hNTs Inhibitor on Cytotoxic Efficacy of GEM and GEM-BSA NPs in MIAPaCa-2 and PANC-1 Cells

Samples	MIAPaCa-2		PANC-1	
	IC_{50}	Relative resistance	IC_{50}	Relative resistance
GEM-BSA NPs	4.79 ± 0.17	-	5.21 ± 0.26	-
GEM	11.57 ± 0.53	-	11.76 ± 0.74	-
GEM-BSA NPs + dipyridamole	5.18 ± 0.20	1.08	5.14 ± 0.35	0.98
GEM + dipyridamole	101.16 ± 8.47	8.74	109.13 ± 7.36	9.27
Values are presented as mean ± SD (n = 3)				

Cytotoxicity studies

In-vitro cell cytotoxicity of GEM and GEM-BSA NPs were evaluated on MIA-PaCa 2 and PANC-1 cell lines, which revealed significantly enhanced cytotoxicity of GEM-BSA NPs as compared to free GEM in both time and concentration dependent manner **(**Fig. 7 A, B and C). A prevailing time dependent cellular inhibition was shown in case of GEM-BSA NPs.

Fig. 7

Dose-dependent cytotoxicity profile of GEM and GEM-BSA NPs in MIA-PaCa 2 and PANC-1 cell lines after (**a**) 24 (**b**) 48 and (**c**) 72 h treatment; (**d**) 8-OHdG levels in cells treated with free GEM and GEM–BSA NPs in (*a*) MIA-PaCa 2 and (*b*) PANC-1 cell lines.

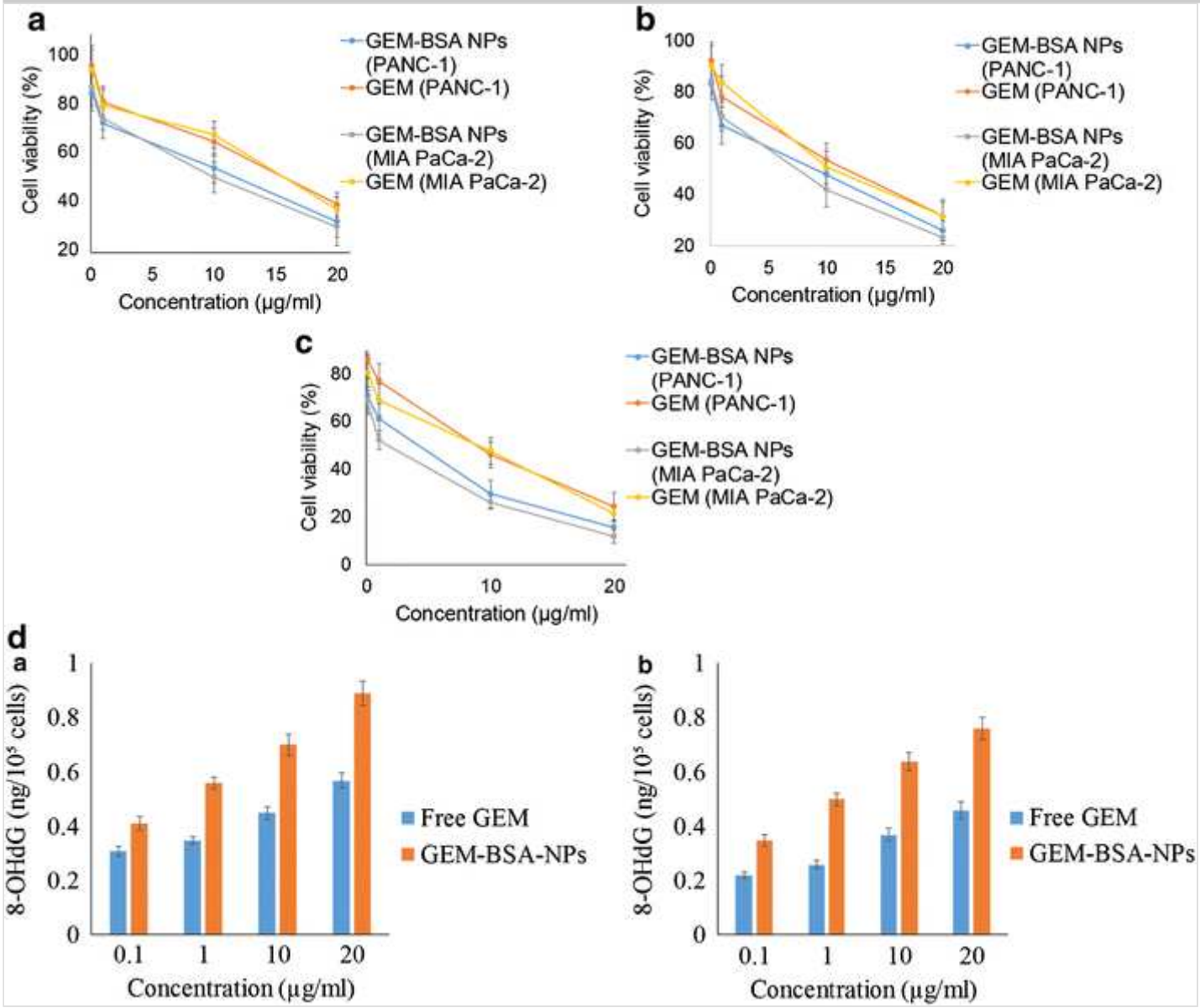

DNA damage assay

The DNA damage analysis affirmed that, the observed cytotoxicity of free GEM and GEM-BSA NPs is facilitated by DNA damage. Significant levels of 8-OHdG ($p < 0.001$) were observed in case of GEM-BSA NPs as compared to GEM (Fig. 7 D).

Annexin V apoptosis assay

The observed results of cytotoxicity and DNA damage assay were further confirmed by the apoptosis assay (Fig. 8). GEM–BSA NPs demonstrated higher apoptotic index as compared with free GEM in both MIA-PaCa-2 and PANC-1 pancreatic cancer cell lines. The apoptotic index in case of GEM was 0.44 and 0.39, while in case of GEM-BSA NPs, the apoptosis index was found to be 0.81 and 0.74, against MIA-PaCa2 and PANC-1 cell lines, respectively.

Fig. 8

Apoptosis assay of GEM (**a**) and GEM-BSA NPs (**b**) against MIAPaCa-2 and PANC-1 cells; (*a*) green channel depicts the fluorescence from carboxy fluorescein (cell viability marker dye); (*b*) red channel depicts fluorescence from Annexin Cy3.18 conjugate (cell apoptosis marker dye) (*c*) represents the overlay image whereas (*d*) depicts the differential contrast image of representative cells. The apoptotic index has been measured as the ratio of fluorescence intensity from the red channel to that of the green channel. The fluorescence intensities of the images were measured using Image J software, U. S. National Institutes of Health, Bethesda, Maryland, USA, http://imagej.nih.gov/ij/ .

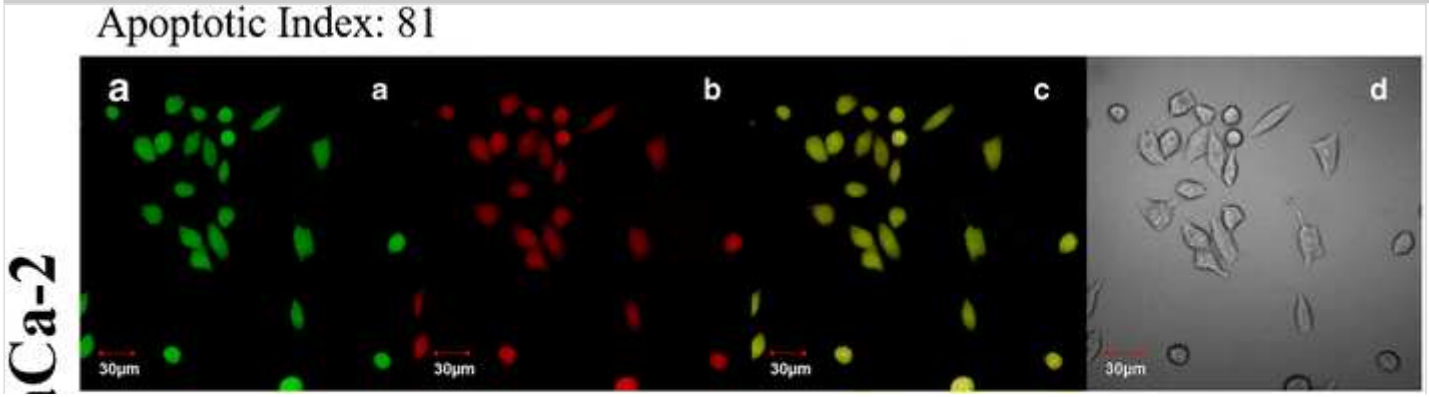

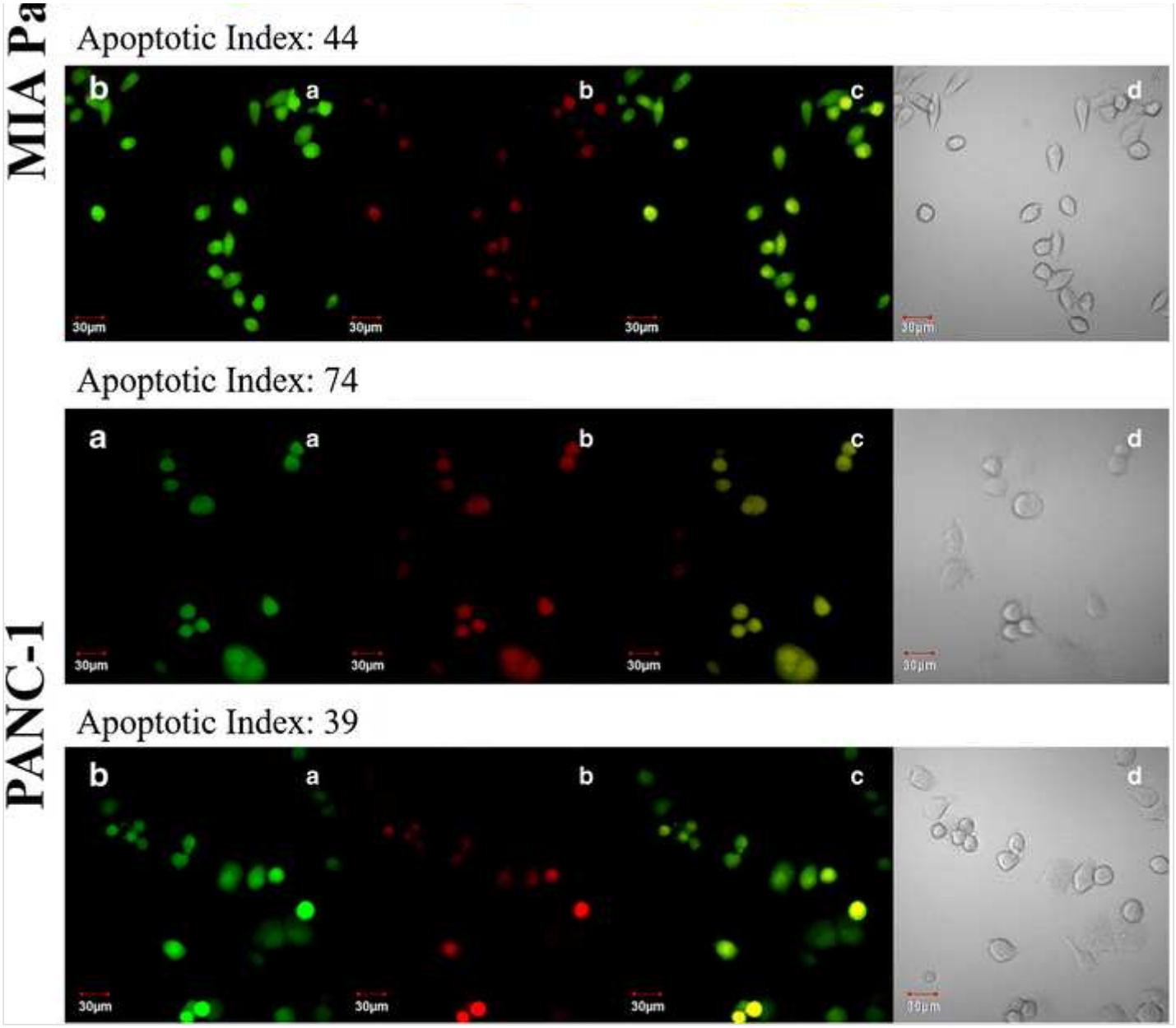
MIA Pa
Apoptotic Index: 44
b
a
b
c
d
30µm
Apoptotic Index: 74
PANC-1
a
a
b
c
d
30µm
Apoptotic Index: 39
b
a
b
c
d
30µm

DISCUSSION

Despite promising therapeutic potential in various cancers the clinical application of GEM has been hindered due owing to its rapid deamination via cytidine deaminase (CDA), high hepatic clearance, poor physiochemical properties and pharmacokinetic profile (24). In the present study GEM-BSA NPs were designed with the aim to overcome these limitations and to enhance the therapeutic efficacy of GEM. To develop GEM-BSA NPs, first GEM-BSA conjugate was synthesized by using EDC/NHS coupling reaction. The amide bond formed between the GEM and BSA is expected to enhance the stability of GEM against CDA mediated degradation or metabolism of GEM into inactive uracil metabolite (25). Degree of modification was tested by using TNBS method which was found to be 11.44%, i.e., 20.33 μM, GEM was conjugated with the equimolar concentration of amine groups in the BSA. Ratio of GEM and BSA was found to be ~6.7:1 (20.33 μM:3.0303 μM; 7 mol of GEM conjugated with 1 mol of BSA), which confirms the efficient conjugation of GEM and BSA. In line with TNBS method, MALDI-TOF further confirmed the formation of ~7.17 mol of modified GEM. Gel electrophoresis further confirmed the higher molecular weight of GEM-BSA conjugate (lane 3) in comparison with free BSA (lane 2). Elemental analysis showed an increase in the percent nitrogen and carbon in the GEM-BSA conjugate in comparison with BSA and could be due to the additional 3 nitrogen atoms (1 in $–NH_2$ group and 2 in pyrimidine ring) and carbon (sugar and pyrimidine ring) present in GEM structure. Furthermore, the sulphur content was found to be same in case of both BSA and GEM-BSA conjugate which could be due to the absence of sulphur in GEM.

BSA exhibits intrinsic fluorescence when the tryptophan moieties (two residues present at position 134, and 212 in subdomain IB and subdomain IIA, respectively) are excited at 280 nm, while, the emission spectra are recorded with in the range of 300–400 nm. The intrinsic fluorescence of BSA is very sensitive to the surrounding horizons and demonstrates significant quenching when influenced by the presence of quencher. (26) Thus, on conjugation of GEM with BSA, the micro environment of the tryptophan is expected to be altered and about ~2.4-fold decrease in fluorescence intensity of BSA may be ascribed to the conjugation of GEM with BSA. GEM conjugation with BSA resulted in significant changes in the structural conformation in case of ß-sheets and turns, however, no significant difference was noticed in the levels of α-helix. In addition to the SPARC (Secreted Protein, Acidic and Rich in Cysteine) protein, responsible to engulf the native albumin, the cancer cells also express gp18 and gp30 receptors which specifically bind to conformationally-modified albumin leading to higher cellular uptake of altered albumin (27,28). Thus, the conformational changes noticed following the conjugation may result in to preferentially enhanced uptake of GEM-BSA NPs by cancer cells.

BSA is primarily composed of helical structure formed through several intramolecular hydrogen bonds between oxygen (of carboxyl group) and hydrogen atom of every fourth peptide bond. Thus, any alteration in the conformation due to conjugation will lead to structural changes in the helical structure of BSA molecule. Raman spectroscopy analyse various bands of protein such as amide I band (α-helical conformation from peptide C = O stretching vibration, at ~1650 cm^{-1}), amide III band (C-N bond stretching and in-plane N-H bond bending) and skeletal vibration regions (29). The changes in Raman spectra of BSA on conjugation demonstrated an increase and decrease in the intensity of the amide III region (at 1200–1300 cm^{-1}) and skeletal region (at 900–1000 cm^{-1}), respectively. The increase and decrease in intensity at 1246 and 934 was found to be associated with upsurge in random coil conformations and with loss of α-helical content, respectively, demonstrating change in conformation of BSA on conjugation with GEM. (30) The results obtained by Raman spectroscopy was found to be in line with the quantitative results obtained via CD spectroscopy.

The thermal behaviour of the developed conjugate was estimated via DSC and TGA analysis. Endothermic peak of GEM in the physical mixture of BSA and GEM was found to be unaltered due to the presence of crystalline structure, corresponding to the melting point of GEM (~273°C). GEM-BSA conjugate demonstrated loss of endothermal peak, indicating the absence of crystalline structure following the conjugation of GEM with BSA. Furthermore, the presence of GEM in an amorphous form within GEM-BSA conjugate was evaluated by TGA. TGA curve demonstrated the presence of two prominent decomposition steps in both case of BSA and GEM-BSA conjugate. The first stage of the moderate decomposition observed from room temperature to ~110°C could be attributed to the loss of water or absorbed moisture (31). After a short plateau phase the TG curve demonstrates second weight loss which corresponds to the decomposition of BSA and GEM-BSA conjugate. Second weight loss in case of GEM-BSA started at ~160°C as compared to BSA (~235°C). Moreover, the TG results demonstrate a higher weight loss percentage of GEM-BSA conjugate than that of the BSA at the same temperature. The difference in the two-step degradation behaviour or percentage of total mass loss of the BSA and GEM-BSA confirmed the conjugation of GEM with BSA.

Contact angle is one of the most widely used techniques for comparative evaluation of material by estimating the wettability, an inherent property, of the material. GEM-BSA conjugate (contact angle 115.15 ± 2.72) exhibited stronger interaction with the water droplet indicating significantly higher wettability as compared to BSA (contact

angle 70.13 ± 3.57). This appreciation of the wettability in case of conjugate might be ascribed to the enhanced hydrophilicity of the BSA following the covalent conjugation with hydrophilic GEM.

GEM-BSA NPs were prepared by high pressure homogenization to further potentiate the cytotoxic effect of GEM-BSA conjugate by selectively delivering high drug level to the desired site of action. Moreover, unmodified BSA NPs were also prepared to evaluate the effect of conjugation on NPs development. To overcome the poor storage stability of NPs in suspension form, freeze dried form was prepared by using mannitol (5% *w*/*v*) as cryoprotectant. Minimal changes in the quality attributes were found in case of mannitol, which might be ascribed due to development of stable network of cryoprotectants with NPs. The obtained results were found to be in accordance with earlier reports in which Mannitol has been reported to provide sufficient stability against the stress during the freeze drying process (32). Excellent storage stability at accelerated storage conditions could also be ascribed to strong network of cryoprotectants around the NPs.

The GEM-BSA NPs exhibited relatively lower ZP (−19.2 ± 1.41 mV) as compared to BSA NPs (139.3 ± 6.6 nm and −34.5 ± 1.65) and could be attributed to the decrease amino groups following the conjugation of GEM with BSA (33). AFM and SEM analysis further confirmed the formation of spherical nanoparticles with smooth surface and also the results were found to be in good correlation with the results of zeta sizer. The presence of GEM within BSA nanoparticles was confirmed by PXRD, demonstrated loss of characteristic peaks of GEM in the PXRD spectra of GEM-BSA NPs, suggesting existence of amorphous form of GEM when conjugated with BSA and further development of NPs.

Furthermore, to evaluate the release profile of the GEM from the GEM-BSA NPs, *in-vitro* hydrolysis study was evaluated at pH 7.4 and 5.5 with and without enzymes to simulate systemic circulation and tumour microenvironment, respectively. The rate of GEM release from nanoformulation was found to be higher at pH 5.5 in presence of proteases, which could be due to the controlled scission of amide bond amid GEM and BSA and degradation by the enzyme.

The drug delivery potential of GEM-BSA NPs was evaluated via assessing the cell uptake in MIA-PaCa 2 and PANC-1 cells. The results revealed a significantly enhaced uptake of C-6 loaded GEM-BSA nanoparticles as compared to free C-6, suggesting efficient cellular retention of NPs in cancer cells and expected to reduce the dose

and frequency in clinical setting. This enhanced cellular uptake was suggestive of additional cellular internalization pathways involved in NPs uptake. Thus, to understand the reliance of energy dependent cellular uptake of NPs, the cells were incubated with C-6 loaded GEM-BSA NPs at 4°C and in the presence of SA. A significant reduction of fluorescence intensity was noticed at 4°C (supplementary information), which might be due to the lower metabolic activity and poor membrane fluidity of the cells at this temperature (34,35). Pre-incubation with SA also significantly reduced the C-6 fluorescence intensity and could be ascribed to the SA mediated ATP depletion within the cells. The fluorescence inhibition, in case of pre-incubation with SA, was found to be partial as compared to the intensity at 4°C, and could be assigned to the presence of consumption of exogenous ATP. Thus, the cell uptake inhibition of NPs at 4°C and in the presence of SA clearly suggests involvement of energy-dependent active endocytosis process (36).

Different mechanisms of cellular uptake of nanoparticle internalization have been described such as, clathrin mediated endocytosis, caveolae mediated endocytosis, clathrin and caveolae independent and macropinocytosis (37,38). To understand the specific endocytosis facilitated cell uptake mechanisms, the cells were incubated with C-6 loaded GEM-BSA NPs in the presence of pharmacological inhibitors that suppress the activity of specific cellular uptake pathways such as genistein (caveolae uptake inhibitor), chlorpromazine (clathrin uptake inhibitor) and a combination of both chlorpromazine and genistein. A significant retardation of the fluorescence in the presence of clathrin mediated endocytosis inhibitors while, a slight decrease in fluorescence in case of caveolae uptake inhibitor indicate the involvement of both the cellular uptake pathways being clathrin mediated endocytic cellular uptake as primary uptake mechanism.

LysoTracker Red dye mediated subcellular trafficking route of NPs was employed to verify the efficient internalization and to explore the fate of nanoparticles after cell uptake (39). Fig. 6 demonstrates negligible red fluorescence of the LysoTracker Red in case of control cells and cells incubated with free GEM, while significantly enhanced red fluorescence was found, on incubation of C-6 loaded NPs, which clearly demonstrates radical increase in the lysosome formation. Moreover, the green fluorescence of C-6 loaded NPs was found to be co-localized with the red fluorescence from LysoTracker Red (yellow fluorescence in the overlays) suggesting selective endocytic uptake of NPs through endo-lysosomes pathway (40). The results further confirmed the findings of cell uptake and internalization study, as NPs were following clathrin and caveolae mediated endocytic

pathway conclude in endo-lysosome or golgi subcellular structures and endocytic reticulum by-passing the endo-lysosomal pathway, respectively (41).

MIA-PaCa 2 and PANC-1 cell cytotoxicity experiments demonstrated that GEM retained its antitumor efficacy even after conjugation with BSA, which was found to be in line with our earlier reports (6,14). GEM-BSA NPs exhibited significantly higher concentration and time dependent cell cytotoxicity as compared to free GEM. The observed results could be attributed to enhanced cellular uptake (via clathrin mediated endocytosis) of GEM-BSA NPs and improved physicochemical properties and enhanced stability against CDA of GEM on conjugation with BSA. In contrast, relatively lower cytotoxicity was found in case of GEM, which could be due to rapid metabolism and lower cellular uptake (via nucleoside transporters; hNTs) of free GEM (42).

GEM due to its hydrophilic nature requires specialized hNTs (human equilibrative nucleoside transporters, hENTs and human concentrative nucleoside transporters, hCNTs) to cross the hydrophobic cellular membrane, therefore, responsible for the clinical sensitivity towards GEM treatment and development of resistant tumours (43). Thus, the effect of hNTs levels on the cell cytotoxicity of GEM and GEM-BSA NPs was evaluated in two different cell lines. The IC_{50} of GEM was drastically increased to 8.74 and 9.27 folds in case of MIA-PaCa 2 (GEM sensitive) and PANC-1 (GEM resistant), indicating that the GEM transport was mediated through hNTs. On the contrary, the activity of the GEM-BSA NPs was found to be unaltered in case of both the cell lines, which further confirms that the cell uptake of NPs was independent of hNTs and can be an effective approach in overcoming drug resistance in cancer, which is found to be in line with the previously published data (44).

The results of cell cytotoxicity observed in the MTT assay were further corroborated by the apoptosis studies. Quantitative and qualitative analysis of apoptosis induced by the treatment of GEM and GEM-BSA NPs was performed by DNA damage and Annexin-V analysis. DNA damage is one of the primary mechanism of GEM, which triggers the apoptotic signalling cascade (45). Significantly higher levels of 8-OHdG was observed when the cells were treated with GEM-BSA NPs in comparison with free GEM, confirmed that the activity of GEM was not lost following the conjugation with BSA and was efficiently transported to the nuclear fraction after endosomal lysis from the BSA. Moreover, the Annexin-V apoptosis results were found to be in line with the DNA damage assay, which demonstrates remarkably higher levels of the apoptotic index in case of treatment with GEM-BSA NPs in both GEM sensitive as well as resistant cell lines, which could be due to cumulative effect of higher

cell uptake or internalization and further its retention of NPs within MIA-PaCa 2 and PANC-1 cells and enhanced stability on conjugation of GEM with BSA as compared to that of free GEM alone.

CONCLUSION

In the present report, GEM and BSA macromolecular bioconjugate has been developed by covalently attaching GEM with BSA and further processed to form nanoparticles by using high pressure homogenization technique. Effective conjugation of GEM with BSA resulted into the transformation of physicochemical properties of GEM and increased stability thereof. GEM-BSA NPs exhibited remarkably higher cellular uptake via clathrin mediated endo-lysosomal pathway. Furthermore, GEM-BSA NPs demonstrated significantly higher IC_{50} value of 4.79 ± 0.17 and 5.21 ± 0.26 and apoptotic index of 0.81 and 0.74 in both MIA-PaCa 2 and PANC-1 cell lines, respectively. The present report offers an additional research horizon of drug macromolecule conjugates to overcome the limitations of drug molecules like GEM. Furthermore, the research strategy can be efficiently extended for the potent drugs (hydrophobic as well as hydrophilic), with limited clinical efficacy. Detailed pharmacokinetic and pharmacodynamics studies of the GEM-BSA NPs are underway which will be reported in due course.

ACKNOWLEDGMENTS AND DISCLOSURES The authors are thankful to the Director NIPER, James Graham Brown Cancer Center (University of Louisville, KY, USA) and Strathclyde Institute of Pharmacy & Biomedical Sciences (University of Strathclyde, Glasgow, U.K.) for necessary infrastructure and facilities. Varun Kushwah is also grateful to the Council of Scientific and Industrial Research (CSIR), GOI, New Delhi, United States-India Educational Foundation, New Delhi and Commonwealth commission in the UK for providing research funding and fellowships. He was the 2016–17 Fulbright-Nehru Doctoral and 2015–16 Commonwealth Split-site PhD research fellow at University of Louisville, Louisville, KY and University of Strathclyde, Glasgow, U.K., respectively.

Electronic supplementary material

ESM 1

(DOCX 992 kb)

REFERENCES

1. von der Maase H, Hansen S, Roberts J, Dogliotti L, Oliver T, Moore M, et al. Gemcitabine and cisplatin versus methotrexate, vinblastine, doxorubicin, and cisplatin in advanced or metastatic bladder cancer: results of a large, randomized, multinational, multicenter, phase III study. J Clin Oncol. 2000;18(17):3068–77.

2. Moore MJ, Tannock IF, Ernst DS, Huan S, Murray N. Gemcitabine: a promising new agent in the treatment of advanced urothelial cancer. J Clin Oncol. 1997;15(12):3441–5.

3. Zisman A, Ng C-P, Pantuck AJ, Bonavida B, Belldegrun AS. Actinomycin D and gemcitabine synergistically sensitize androgen-independent prostate cancer cells to Apo2L/TRAIL-mediated apoptosis. J Immunother. 2001;24(6):459–71.

4. Bernardo G, Cuzzoni Q, Strada MR, Bernardo A, Brunetti G, Jedrychowska I, et al. First-line chemotherapy with vinorelbine, gemcitabine, and carboplatin in the treatment of brain metastases from non-small-cell lung cancer: a phase II study. Cancer Investig. 2002;20(3):293–302.

5. Vrignaud S, Benoit J-P, Saulnier P. Strategies for the nanoencapsulation of hydrophilic molecules in polymer-based nanoparticles. Biomaterials. 2011;32(33):8593–604.

6. Das M, Jain R, Agrawal AK, Thanki K, Jain S. Macromolecular bipill of gemcitabine and methotrexate facilitates tumor-specific dual drug therapy with higher benefit-to-risk ratio. Bioconjug Chem. 2014;25(3):501–9.

7. Achiwa H, Oguri T, Sato S, Maeda H, Niimi T, Ueda R. Determinants of sensitivity and resistance to gemcitabine: The roles of human equilibrative nucleoside transporter 1 and deoxycytidine kinase in non-small

cell lung cancer. Cancer Sci. 2004;95(9):753–7.

8. Duncan R. Polymer conjugates as anticancer nanomedicines. Nat Rev Cancer. 2006;6(9):688–701.

9. Duncan R, Gac-Breton S, Keane R, Musila R, Sat Y, Satchi R, et al. Polymer–drug conjugates, PDEPT and PELT: basic principles for design and transfer from the laboratory to clinic. J Control Release. 2001;74(1):135–46.

10. Khandare J, Minko T. Polymer–drug conjugates: progress in polymeric prodrugs. Prog Polym Sci. 2006;31(4):359–97.

11. Pasut G, Canal F, Dalla Via L, Arpicco S, Veronese FM, Schiavon O. Antitumoral activity of PEG–gemcitabine prodrugs targeted by folic acid. J Control Release. 2008;127(3):239–48.

12. Neff T, Blau C. Forced expression of cytidine deaminase confers resistance to cytosine arabinoside and gemcitabine. Exp Hematol. 1996;24(11):1340–6.

13. Sugiyama E, Kaniwa N, Kim S-R, Kikura-Hanajiri R, Hasegawa R, Maekawa K, et al. Pharmacokinetics of gemcitabine in Japanese cancer patients: the impact of a cytidine deaminase polymorphism. J Clin Oncol. 2006;25(1):32–42.

14. Jain S, Jain R, Das M, Agrawal AK, Thanki K, Kushwah V. Combinatorial bio-conjugation of gemcitabine and curcumin enables dual drug delivery with synergistic anticancer efficacy and reduced toxicity. RSC Adv. 2014;4(55):29193–201.

15. Chitkara D, Mittal A, Behrman SW, Kumar N, Mahato RI. Self-assembling, amphiphilic polymer–gemcitabine conjugate shows enhanced antitumor efficacy against human pancreatic adenocarcinoma. Bioconjug Chem. 2013;24(7):1161–73.

16. Neil I. Nab technology: A drug delivery platform utilising endothelial gp60 receptor-based transport and tumour-derived SPARC for targeting. Drug Deliv. Rep. 2017: 37-41.

AQ2

17. Stevis PE, Deecher DC, Suhadolnik L, Mallis LM, Frail DE. Differential effects of estradiol and estradiol-BSA conjugates. Endocrinology. 1999;140(11):5455–8.

18. Kim TH, Jiang HH, Youn YS, Park CW, Tak KK, Lee S, et al. Preparation and characterization of water-soluble albumin-bound curcumin nanoparticles with improved antitumor activity. Int J Pharm. 2011;403(1):285–91.

19. Hoang B, Ernsting MJ, Roy A, Murakami M, Undzys E, Li S-D. Docetaxel-carboxymethylcellulose nanoparticles target cells via a SPARC and albumin dependent mechanism. Biomaterials. 2015;59:66–76.

20. Lai SK, Hida K, Man ST, Chen C, Machamer C, Schroer TA, et al. Privileged delivery of polymer nanoparticles to the perinuclear region of live cells via a non-clathrin, non-degradative pathway. Biomaterials. 2007;28(18):2876–84.

21. Khare V, Kour S, Alam N, Dubey RD, Saneja A, Koul M, et al. Synthesis, characterization and mechanistic-insight into the anti-proliferative potential of PLGA-gemcitabine conjugate. Int J Pharm. 2014;470(1):51–62.

22. Dora CP, Trotta F, Kushwah V, Devasari N, Singh C, Suresh S, et al. Potential of erlotinib cyclodextrin nanosponge complex to enhance solubility, dissolution rate, in vitro cytotoxicity and oral bioavailability. Carbohydr Polym. 2016;137:339–49.

23. Jain S, Spandana G, Agrawal AK, Kushwah V, Thanki K. Enhanced antitumor efficacy and reduced toxicity of docetaxel loaded estradiol functionalized stealth polymeric nanoparticles. Mol Pharm. 2015;12(11):3871–84.

24. Serdjebi C, Seitz J-F, Ciccolini J, Duluc M, Norguet E, Fina F, et al. Rapid deaminator status is associated with poor clinical outcome in pancreatic cancer patients treated with a gemcitabine-based regimen. Pharmacogenomics. 2013;14(9):1047–51.

25. Chung W-G, Sandoval MA, Sloat BR, Lansakara-P DS, Cui Z. Stearoyl gemcitabine nanoparticles overcome resistance related to the over-expression of ribonucleotide reductase subunit M1. J Control Release. 2012;157(1):132–40.

26. Ghali M. Static quenching of bovine serum albumin conjugated with small size CdS nanocrystalline quantum dots. J Lumin. 2010;130(7):1254–7.

27. Schnitzer J, Bravo J. High affinity binding, endocytosis, and degradation of conformationally modified albumins. Potential role of gp30 and gp18 as novel scavenger receptors. J Biol Chem. 1993;268(10):7562–70.

28. Schnitzer J, Sung A, Horvat R, Bravo J. Preferential interaction of albumin-binding proteins, gp30 and gp18, with conformationally modified albumins. Presence in many cells and tissues with a possible role in catabolism. J Biol Chem. 1992;267(34):24544–53.

29. Bolton BA, Scherer JR. Raman spectra and water absorption of bovine serum albumin. J Phys Chem. 1989;93(22):7635–40.

30. Lin V, Koenig J. Raman studies of bovine serum albumin. Biopolymers. 1976;15(1):203–18.

31. Ahmad MW, Kim CR, Baeck JS, Chang Y, Kim TJ, Bae JE, et al. Bovine serum albumin (BSA) and cleaved-BSA conjugated ultrasmall Gd 2 O 3 nanoparticles: Synthesis, characterization, and application to MRI contrast agents. Colloids Surf A Physicochem Eng Asp. 2014;450:67–75.

32. Zhao D, Zhao X, Zu Y, Li J, Zhang Y, Jiang R, et al. Preparation, characterization, and in vitro targeted delivery of folate-decorated paclitaxel-loaded bovine serum albumin nanoparticles. Int J Nanomedicine.

2010;5(1):669–77.

33. Verbaan F, Oussoren C, Snel C, Crommelin D, Hennink W, Storm G. Steric stabilization of poly (2-(dimethylamino) ethyl methacrylate)-based polyplexes mediates prolonged circulation and tumor targeting in mice. J Gene Med. 2004;6(1):64–75.

34. He C, Hu Y, Yin L, Tang C, Yin C. Effects of particle size and surface charge on cellular uptake and biodistribution of polymeric nanoparticles. Biomaterials. 2010;31(13):3657–66.

35. Murata N, Los DA. Membrane fluidity and temperature perception. Plant Physiol. 1997;115(3):875.

36. Luo Y, Teng Z, Wang TT, Wang Q. Cellular uptake and transport of zein nanoparticles: effects of sodium caseinate. J Agric Food Chem. 2013;61(31):7621–9.

37. Singhal SS, Nagaprashantha L, Singhal P, Singhal S, Singhal J, Awasthi S, et al. RLIP76 Inhibition: A Promising Developmental Therapy for Neuroblastoma. Pharm Res. 2017; 34 (8): 1673–82.
AQ3

38. Kang JH, Jang WY, Ko YT. The Effect of Surface Charges on the Cellular Uptake of Liposomes Investigated by Live Cell Imaging. Pharm Res. 2017; 34(4): 704-17.
AQ4

39. Ma P, Yu H, Zhang X, Mu H, Chu Y, Ni L, et al. Increased Active Tumor Targeting by An αvβ3-Targeting and Cell-Penetrating Bifunctional Peptide-Mediated Dendrimer-Based Conjugate. Pharm Res. 2017;34(1):121–35.

40. Trickler W, Nagvekar A, Dash A. The in vitro sub-cellular localization and in vivo efficacy of novel chitosan/GMO nanostructures containing paclitaxel. Pharm Res. 2009;26(8):1963–73.

41. Chaudhari KR, Kumar A, Khandelwal VKM, Ukawala M, Manjappa AS, Mishra AK, et al. Bone metastasis targeting: a novel approach to reach bone using Zoledronate anchored PLGA nanoparticle as carrier system loaded with Docetaxel. J Control Release. 2012;158(3):470–8.

42. Moysan E, Bastiat G, Benoit J-P. Gemcitabine versus modified gemcitabine: a review of several promising chemical modifications. Mol Pharm. 2012;10(2):430–44.

43. Borbath I, Verbrugghe L, Lai R, Gigot J-F, Humblet Y, Piessevaux H, et al. Human equilibrative nucleoside transporter 1 (hENT1) expression is a potential predictive tool for response to gemcitabine in patients with advanced cholangiocarcinoma. Eur J Cancer. 2012;48(7):990–6.

44. Xu H, Paxton JW, Wu Z. Development of Long-Circulating pH-Sensitive Liposomes to Circumvent Gemcitabine Resistance in Pancreatic Cancer Cells. Pharm Res. 2016;33(7):1628–37.

45. Huang P, Plunkett W. Fludarabine-and gemcitabine-induced apoptosis: incorporation of analogs into DNA is a critical event. Cancer Chemother Pharmacol. 1995;36(3):181–8.